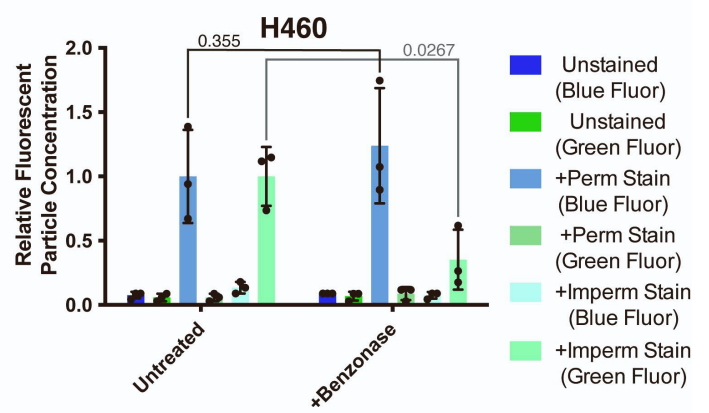
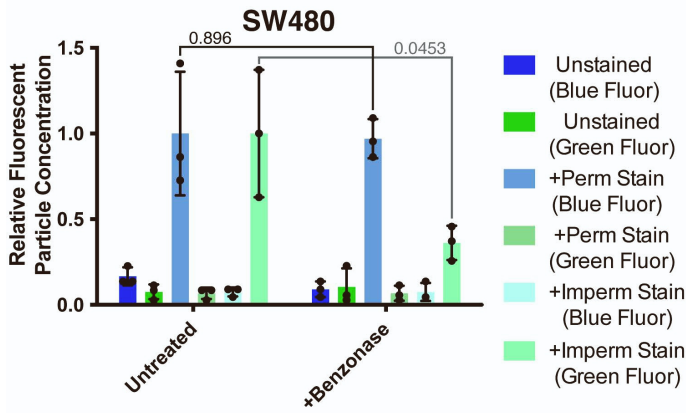
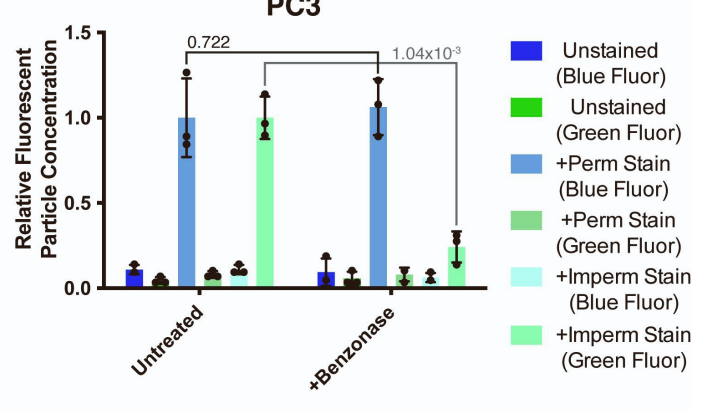
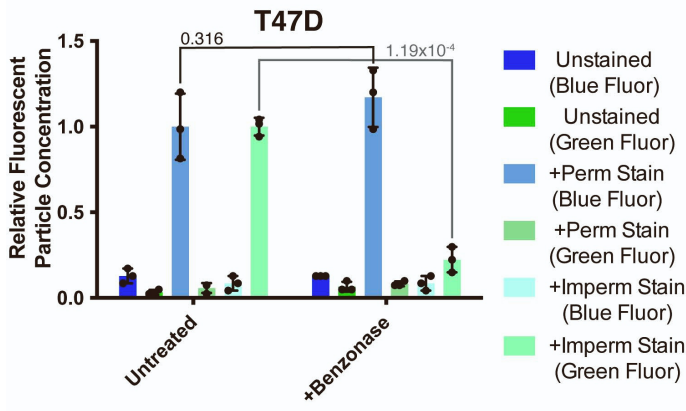
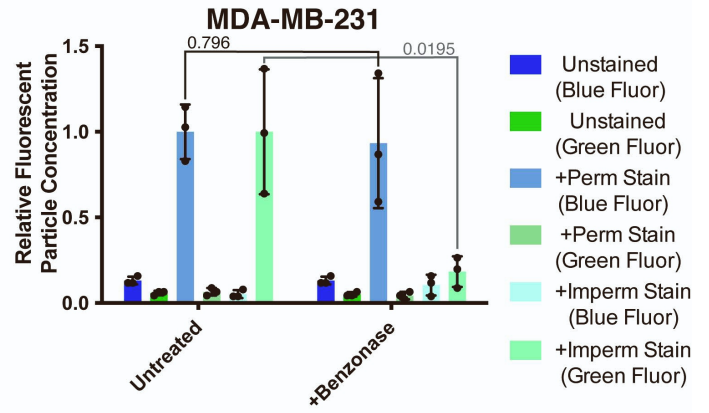
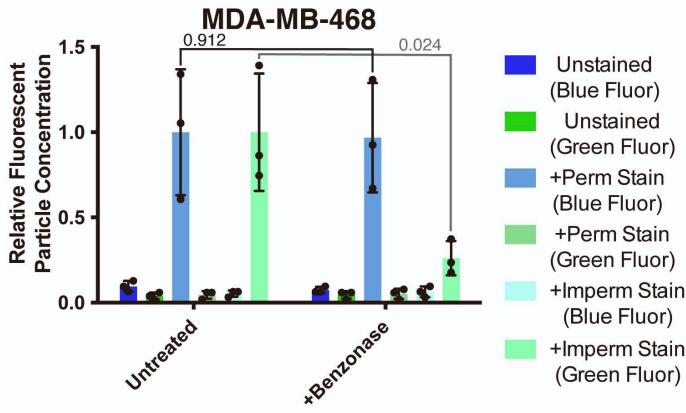
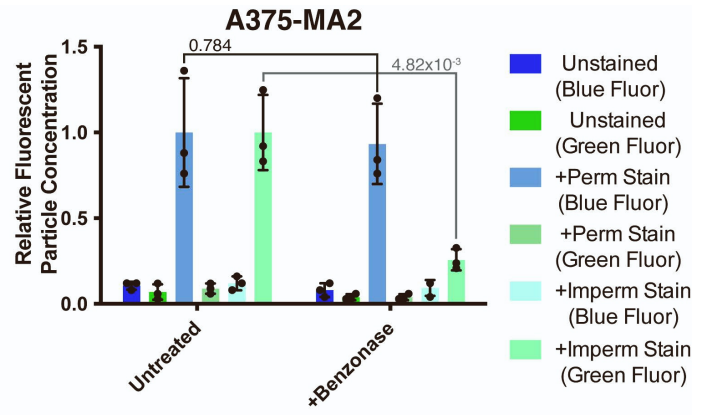
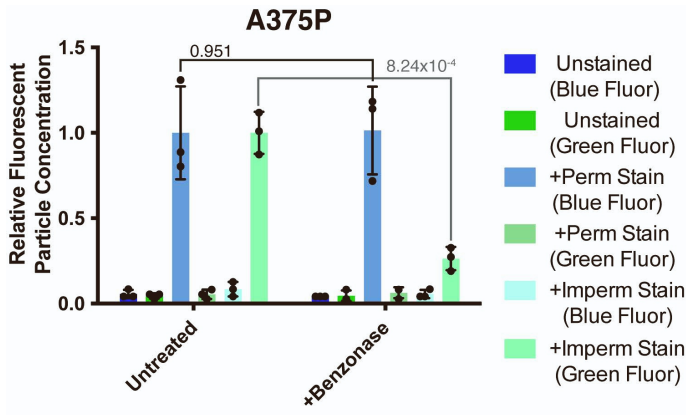


Cell Reports, Volume 38

Supplemental information

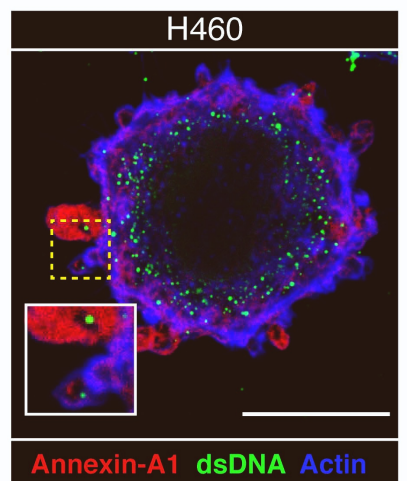
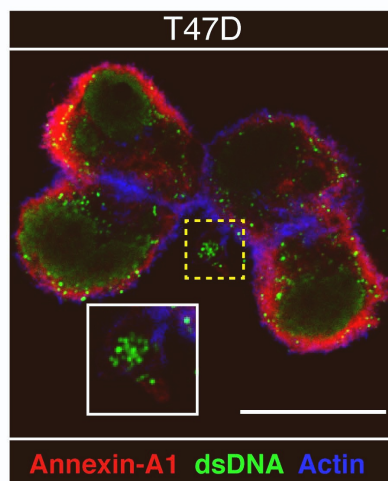
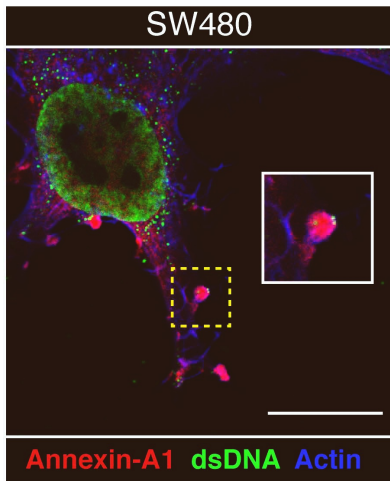
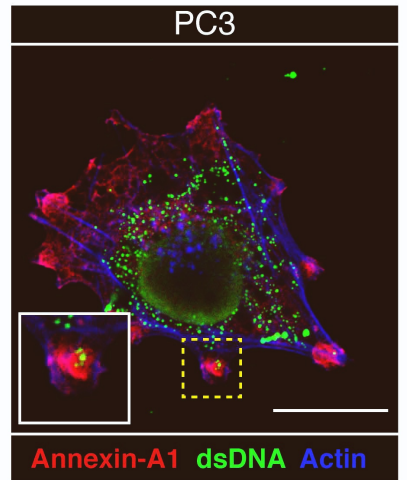
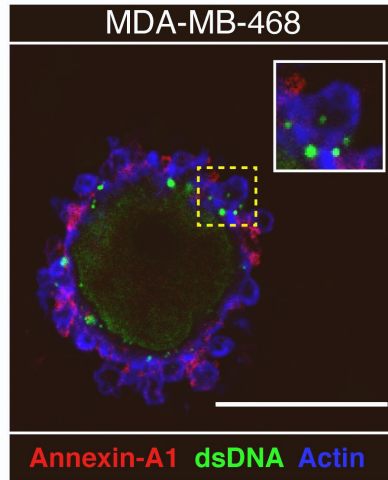
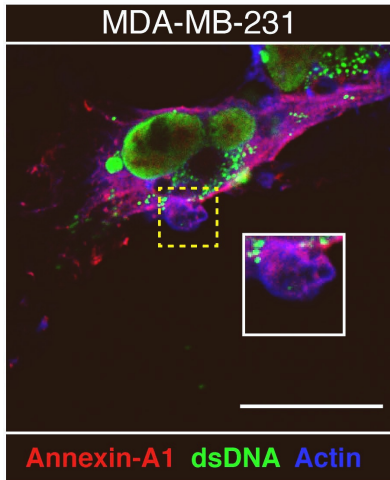
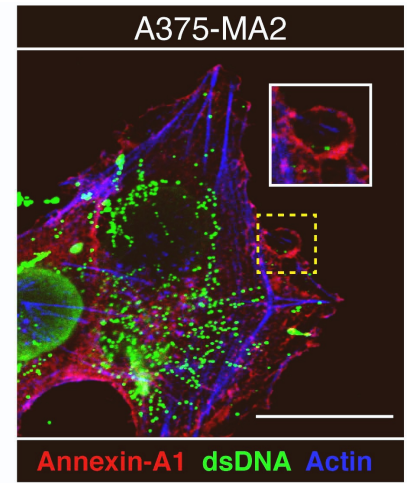
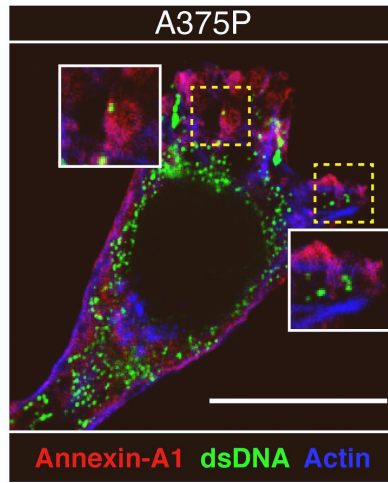
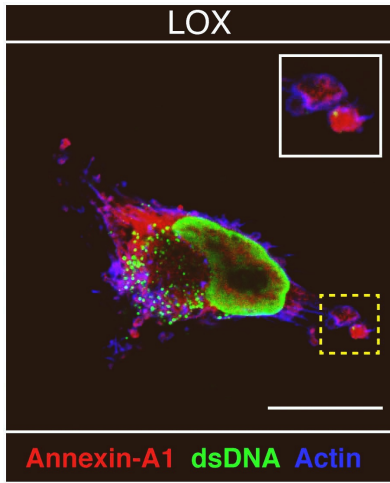
Recruitment of DNA to tumor-derived microvesicles

James W. Clancy, Colin S. Sheehan, Alex C. Boomgarden, and Crislyn D'Souza-Schorey

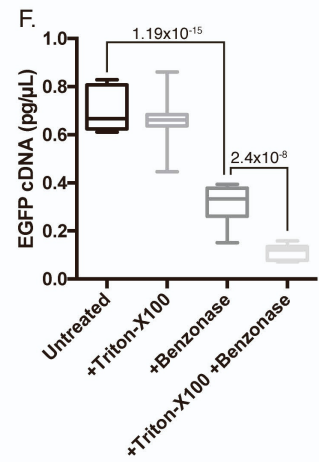
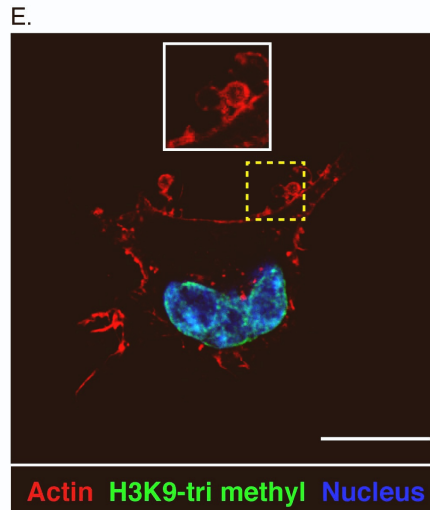
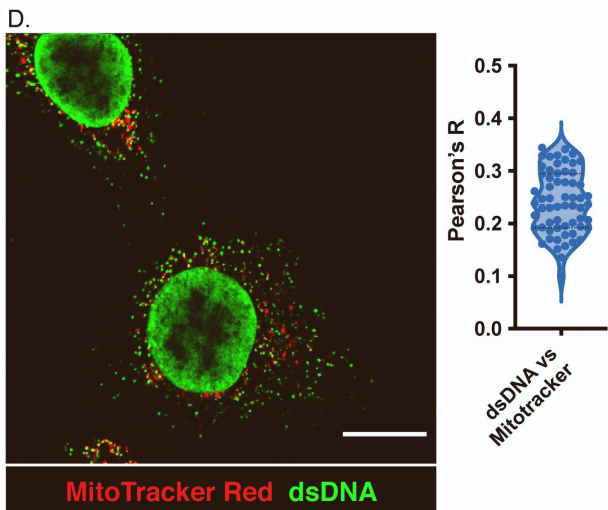
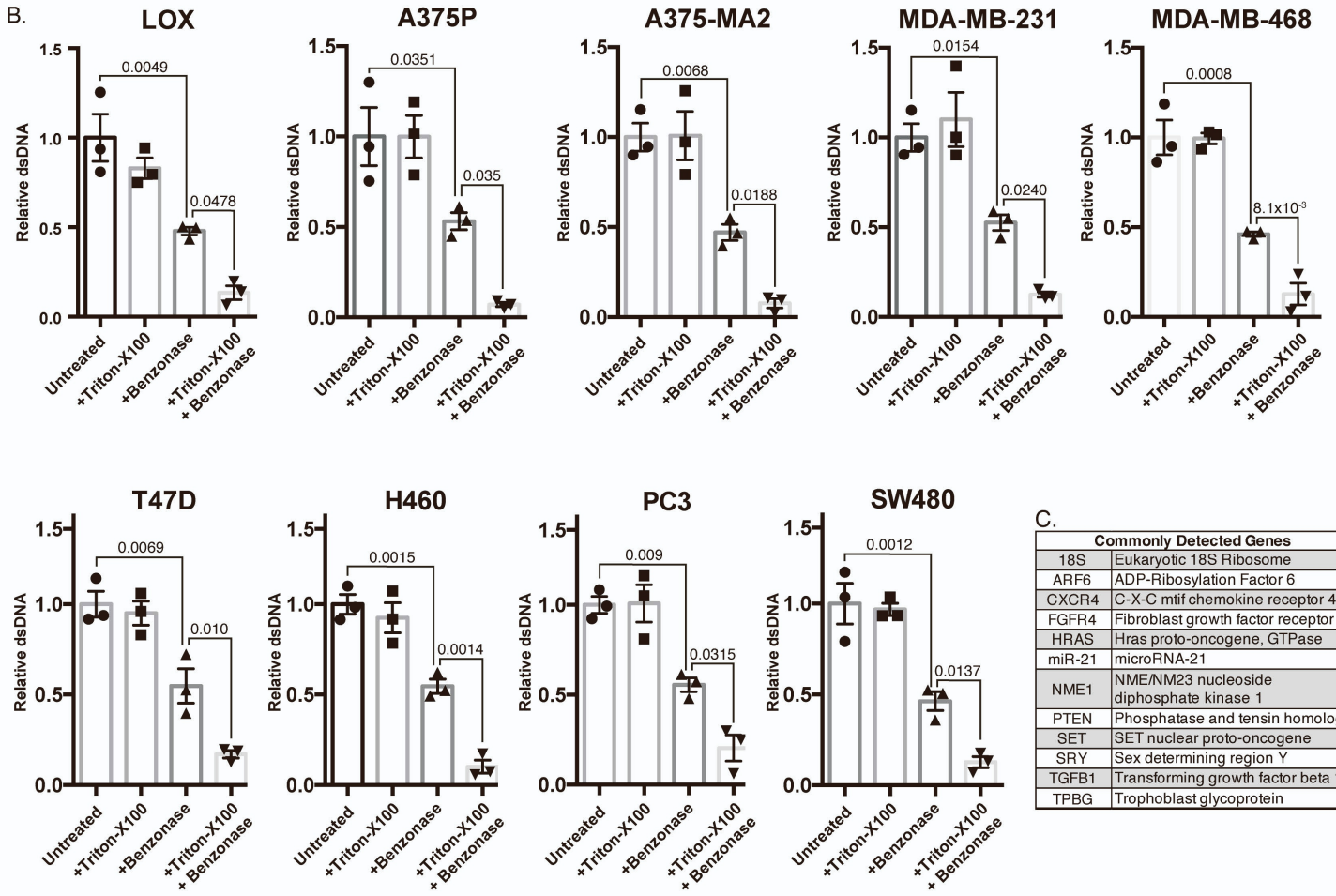
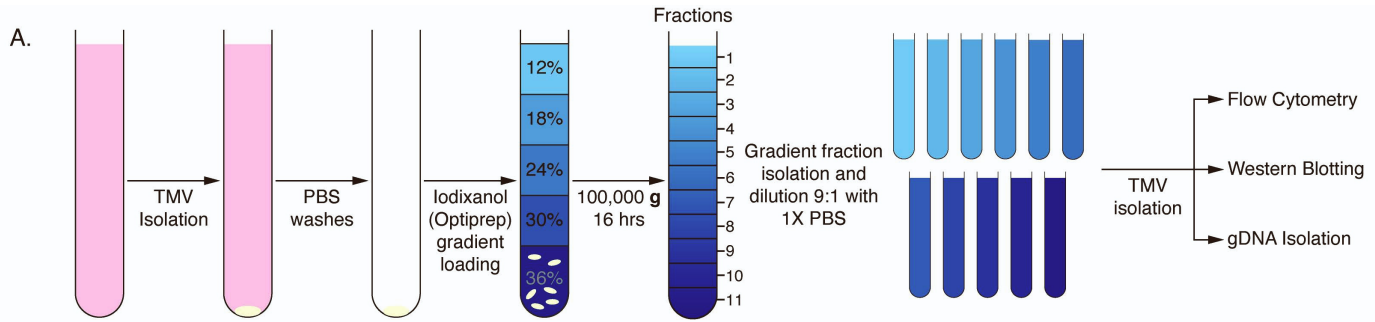


Supplemental Figure 1: Tumor microvesicles from multiple tumor types contain dsDNA, related to Figure 2.

Control or Benzonase treated TMVs isolated from multiple cell lines (as indicated in Figure) were stained with either the cell-permeable blue fluorescing dsDNA dye, NucBlue, or the impermeable green fluorescing dye, NucGreen. Stained TMVs were then analyzed by flow cytometry, demonstrating the significant reduction in the number of vesicles carrying external DNA, stained with the impermeable dye, following treatment with Benzonase. For each cell line, data presented as mean \pm S.E.M. N=3. P values obtained by unpaired, two-tailed t-test for each independent condition.

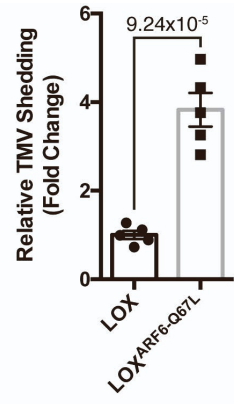
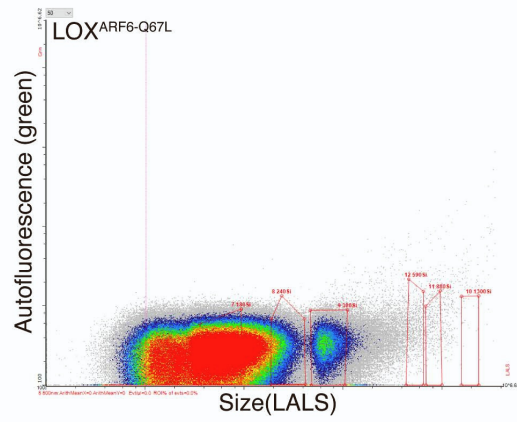
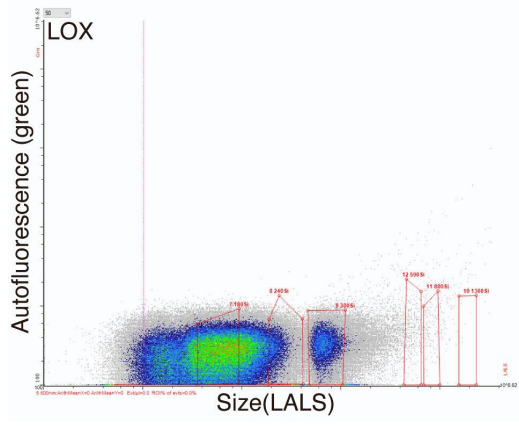


Supplemental Figure 2: Nascent tumor microvesicles from a panel of cell lines contain dsDNA and Annexin-A1 detectable by immunofluorescence, related to Figure 2. Individual cell lines (as indicated in Figure) were plated on glass coverslips and allowed to adhere overnight. The cells were then fixed, stained for Annexin-A1, dsDNA, and the actin cytoskeleton, and the localization of Annexin-A1 and dsDNA examined by confocal microscopy. Scale bars = 15 μm .

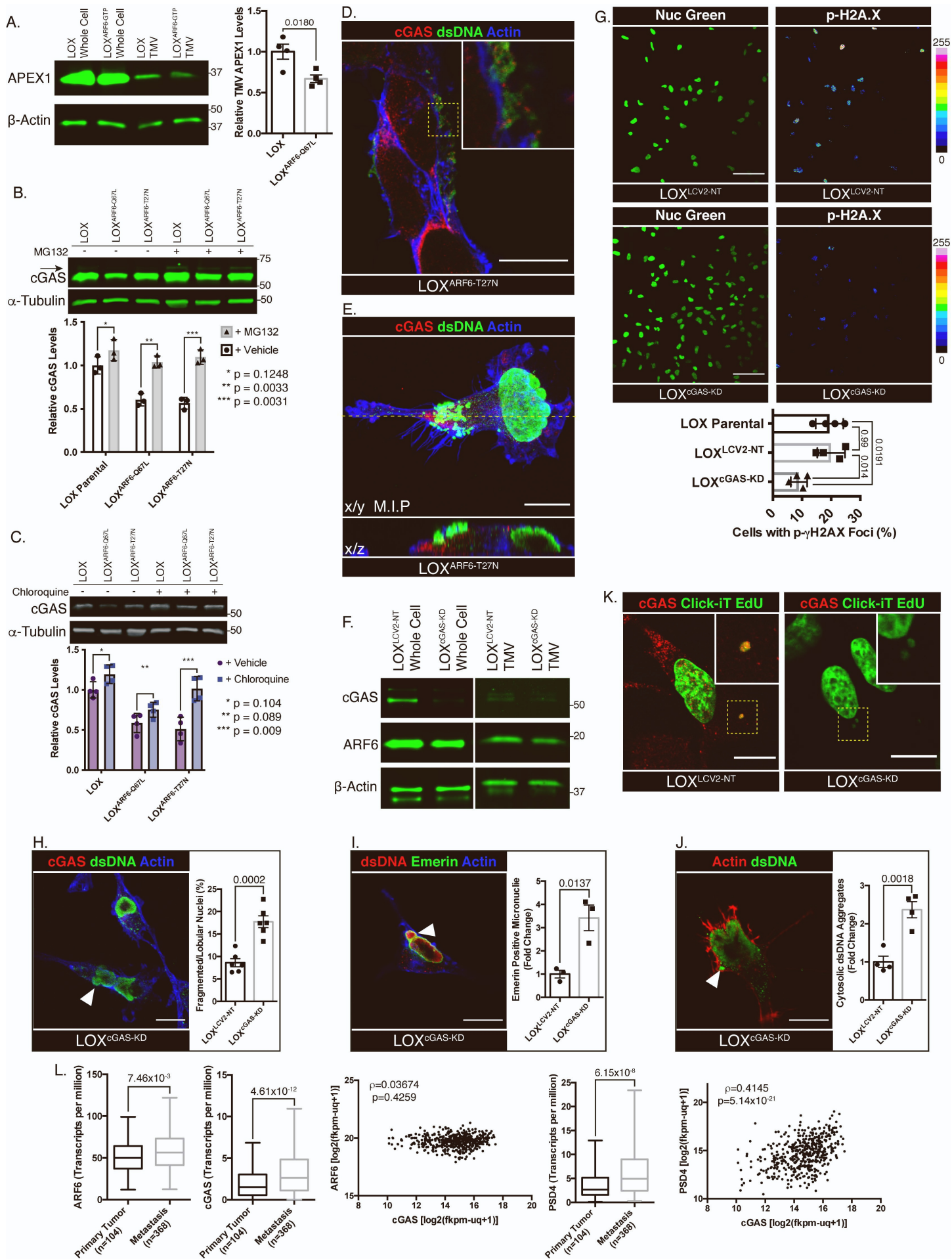


Supplemental Figure 3: TMVs were subjected to high-resolution gradient centrifugation to confirm DNA content, related to Figures 2 and 3.

A. TMVs were isolated as described in methods. The resulting pellet was then used as input for high-resolution Optiprep gradient centrifugation. TMVs were then isolated from the resulting fractions and used for downstream analysis. **B.** TMVs were isolated from individual cell lines as described in methods. Following isolation, TMV pellets were divided evenly into 4 samples, treated as indicated, and their genomic DNA content isolated. Total dsDNA content was then measured by Quant-iT High Sensitivity dsDNA assay. For each cell type, data is presented as mean \pm S.D. N=3. P value obtained by ANOVA with Sidak's correction for multiple comparisons. **C.** LOX melanoma cells in culture were stained with MitoTracker Red according to manufacturer specifications. The cells were then fixed and the dsDNA content stained by immunofluorescence. Only a portion of the punctate extrachromosomal DNA co-labels with mitotracker, as indicated by the plot of Pearson's coefficient R, n=20 cells in each of N=3 biological replicates. **D.** LOX melanoma cells were plated on glass coverslips in preparation for confocal analysis. Immunofluorescent analysis of tri-methyl K9 histone-H3 revealed no detectable signal at the cell periphery where it would be incorporated into budding TMVs. **E.** Exogenous EGFP cDNA was transfected into LOX melanoma cells actively shedding TMVs. Following incubation, TMVs were isolated, treated as indicated, and the dsDNA content isolated. EGFP DNA was then quantified by qRT-PCR. Data presented as mean \pm whiskers indicating max and min values. N=9. P value obtained by ANOVA with Sidak's correction for multiple comparisons. Scale bars = 15 μ m.

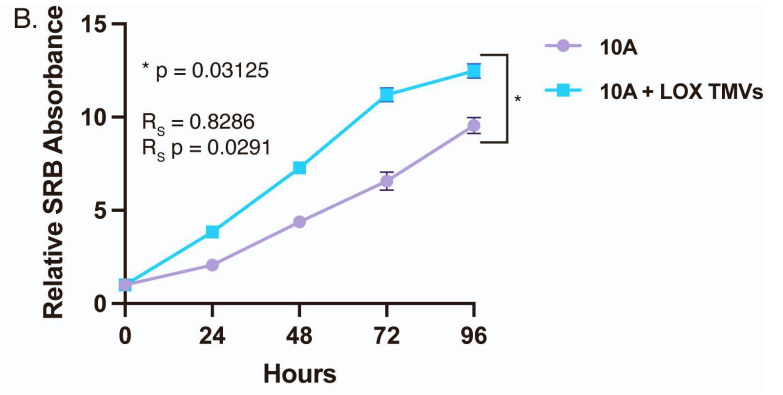
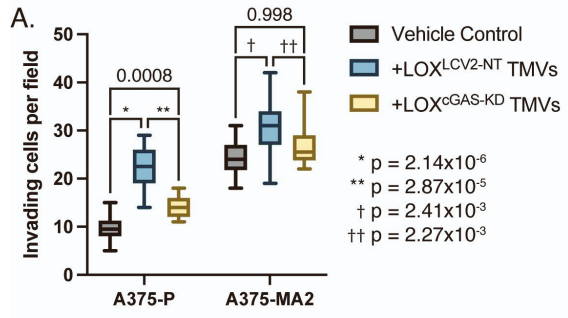


Supplemental Figure 4: ARF6 activation increased TMV shedding from invasive melanoma cells, related to Figure 4. Tumor microvesicles were isolated from conditioned media of an equal number of LOX and LOX^{ARF6-Q67L} melanoma cells as outlined in methods. The isolated TMV pools were then resuspended in 0.1 μ m filtered PBS and analyzed by flow cytometry. Relative total particle counts were then quantified and graphed. Data presented as mean \pm S.D. N=5. P value obtained by unpaired, two-tailed, t-test.



Supplemental Figure 5: ARF6 activation state alters TMV content and dsDNA localization, related to Figure

5. A. Equal amounts of protein lysates from whole LOX and LOX^{ARF6-Q67L} cells and TMVs were separated by SDS-PAGE and APEX1 content examined by western blotting. Relative TMV APEX1 content was quantified and graphed. mean \pm S.D. N=4. P value obtained by unpaired, two-tailed, t-test. **B.** Whole cell lysates from LOX, LOX^{ARF6-Q67L}, and LOX^{ARF6-T27N} cells treated for 6 hours with vehicle control or MG132 were separated by SDS-PAGE. Endogenous cGAS was then examined by western blotting. Relative cGAS levels were quantified and graphed. mean \pm S.D. N=3. P value obtained by unpaired, two-tailed, t-tests. **C.** Equal quantities of protein lysate from LOX, LOX^{ARF6-Q67L}, and LOX^{ARF6-T27N} cells treated for 6 hours with chloroquine and TMVs were separated by SDS-PAGE. cGAS levels were examined by western blotting and quantified by densitometry, presented as mean \pm S.D. N=3. P value obtained by unpaired, two-tailed, t-tests. **D.** Endogenous cGAS and dsDNA were examined by immunofluorescence. Dominant inhibition of ARF6 results in the accumulation of large, intracellular puncta containing both dsDNA and cGAS. Scale bar = 15 μ m. Panel is a short exposure of Figure 5 F to better visualize the colocalization of dsDNA and cGAS (inset). **E.** Immunofluorescent examination of endogenous cGAS and dsDNA in the presence of dominant inhibitory ARF6. Large, intracellular accumulations of dsDNA and cGAS can be seen in the maximum intensity projection, and orthogonal view. Scale bar = 15 μ m. **F.** Equal amounts of protein lysates from whole LOX^{LCV2-NT} and LOX^{cGAS-KD} cells and TMVs were separated by SDS-PAGE and examined by western blotting as indicated. **G.** LOX, LOX^{LCV2-NT} and LOX^{cGAS-KD} cells were plated on glass coverslips, fixed, and stained for p-H2A.X. Cells positive for p-H2A.X foci were counted and quantified. Representative images shown. Scale bar = 100 μ m. Data shown as mean \pm S.E.M. N=4, with at least 300 cells counted per replicate. P value obtained by ANOVA with Sidak's correction for multiple comparisons. LOX^{LCV2-NT} and LOX^{cGAS-KD} cells were plated on glass coverslips, fixed, and stained as indicated. Cells containing nuclear abnormalities (**H**), micronuclei (**I**), or dsDNA aggregates (**J**) were counted and quantified. Representative images shown. Scale bar = 15 μ m. Data shown as mean \pm S.D. Individual biological replicates shown as data points, with at least 300 cells counted per replicate. P value obtained by unpaired, two-tailed, t-tests. **K.** LOX^{LCV2-NT} and LOX^{cGAS-KD} cells were labeled with EdU as indicated in methods. Cells were fixed, and stained as indicated and EdU labeled DNA examined by confocal microscopy. Representative images shown. Scale bar = 15 μ m. **L.** ARF6, cGAS and PSD4 levels were examined in the TCGA data set for cutaneous melanoma. Data was analyzed and statistics calculated using Xena Functional Genomics Explorer (correlation) (Goldman, et al., 2020) or UALCAN (expression) (Chandrashekar, et al., 2017).



Supplemental Figure 6: ARF6 activation state alters TMV content and dsDNA localization, related to Figure

6. A. A375 cells were treated with vehicle control, LOX^{LCV2-NT}, or LOX^{cGAS-KD} TMVs as described in methods. Treated cells were then plated on Matrigel coated transwell inserts and allowed to invade for 16 hours. Invading cells per field of view were counted and quantified and graphed. Data presented as mean \pm S.D., n=25 fields, N=3 biological replicates. P value obtained by ANOVA with Sidak's correction for multiple comparisons. **B.** Incubation with LOX TMVs increases growth rate in MCF-10A cells. Data presented as mean \pm S.D for each time point. N=8. P value obtained by Wilcoxon rank sum test.